Synsint Research Group

Available online at www.synsint.com

Synthesis and Sintering

ISSN 2564-0186 (Print), **ISSN** 2564-0194 (Online)

Research article

Effects of clay and fireclay addition on the properties of magnesia–forsterite–spinel refractories synthesized at different firing temperatures

Esmaeil Salahi [a,*], **Mehran Ghaffari** [a], **A. Faeghinia** [a], **Armin Rajabi** [b]

[a] *Ceramics Department, Materials and Energy Research Center (MERC), Karaj, Iran*

[b] *Department of Mechanical and Manufacturing Engineering, Faculty of Engineering and Built Environment, Universiti Kebangsaan Malaysia, Bangi, 43600, Selangor, Malaysia*

ABSTRACT

This study investigates the effects of adding clay and fireclay on the physical and mechanical properties of magnesia-based refractories such as contraction, bending strength, bulk density, and apparent porosity. Domestic raw materials were used for the preparation of samples fired at 1350, 1450, and 1550 °C for 2 h. Adding clay exhibited no significant effect on the density and porosity, whereas adding fireclay had a remarkable influence on the shrinkage. Nevertheless, the effects of clay and fireclay on the strength of magnesia were unnoticeable. X-ray diffraction results showed that, after firing, the main phase compositions of the samples with clay addition were periclase and forsterite. Adding fireclay led to the synthesis of magnesite spinel, which can be attributed to the high alumina content. Based on scanning electron microscopy, no liquid phase was formed indicating that the sintering was a solid-state evolution with the synthesis of forsterite.

KEYWORDS

Magnesia
Firing
Clay
Fireclay
Refractories
Synthesis

OPEN ACCESS

1. Introduction

Refractory oxides are ceramics that can be employed for elevated-temperature applications [1–5]. Magnesia with a melting point of 2800 °C is a member refractory materials that is broadly used for lining the industrial steel and metallurgical furnaces because of its properties like good slag resistance and superior refractoriness [6–9]. However, the high cost of production of pure magnesia is one of its shortcomings. The appropriate introduction of some cheap components like serpentine, talc, kaolin, and clay is a suitable way to sinter magnesia bricks while maintaining refractory properties and performance [10–13]. It should be mentioned that sintering magnesia refractory materials along with such materials leads to the synthesis of other phases like spinel and forsterite. Sintering mechanisms of magnesia bodies can be enhanced by the formation of aforesaid formed phases [14–16]. Forsterite melts at 1905 °C, which is suitable for the manufacturing of refractory products [17–19]. Also, some characteristics of forsterite are low thermal conductivity, good volume stability, low expansion, and better resistance to high-iron slags compared to magnesia. It is also unreactive to CO_2 and CO gases or water vapor [20–22]. Magnesia exhibits the same behavior against these gases; however, its thermal expansion coefficient (14×10^{-6} K^{-1}) is greater than that of forsterite [23, 24].

In addition to forsterite, the synthesis of spinel results in refractoriness of magnesia bodies [25–27]. Several researchers have done some works about the fabrication of magnesia by synthesis of magnesia–forsterite–spinel bodies. The fine microstructure of sintered forsterite–spinel aggregates was fabricated by the addition of kyanite, sillimanite, and andalusite to magnesia by firing up to 1700 °C [16, 28]. Bodies of fused forsterite–periclase with better resistance were prepared by

* Corresponding author. *E-mail address:* e-salahi@merc.ac.ir (E. Salahi)

Received 25 December 2021; Received in revised form 28 June 2022; Accepted 28 June 2022.

https://doi.org/10.53063/synsint.2022.2280

Table 1. Chemical analysis of raw materials.

Starting materials	Composition (wt%)							
	MgO	Al_2O_3	SiO_2	CaO	Fe_2O_3	Na_2O	K_2O	TiO_2
Magnesite	97.3	0.26	1.3	0.33	0.11	0.26	-	-
Clay	0.05	15.2	75.5	0.28	0.5	0.12	2.5–3	0.56
Fireclay	7.3	43	46	0.29	1.1	0.34	0.28	1.5

smelting dunite with adding brucite, magnesite or sintered periclase [29]. The formation reactions of magnesia achieved from seawater during the isothermal sintering process were examined. To characterize the formation condition of spinel and forsterite, different additives were introduced. Slags of carbon–ferrochrome were utilized to produce the forsterite–spinel bodies. Magnesia was added up to 9 wt% to improve the refractoriness of the produced bodies [30].

The formation of forsterite and spinel by adding Egyptian alum–waste to magnesia was investigated. Egyptian kaolin was employed to study the influence of adding calcined kaolin on the sinterability of dead-burned magnesia. The spinel formation in specimens led to the enhancement of the performance and refractoriness of the produced forsterite parts [31]. Samples with 10─20 wt% kaolin showed good mechanical and high refractory properties as well as high sinterability. It was reported that these samples are suitable to use as a heating zone of cement rotary kilns as well as lining for various sections of steel furnaces. Materials with 30–40 wt% kaolin having restricted refractoriness can be utilized as kiln furniture in ceramic industries or heat exchangers [32]. Forsterite, periclase, and spinel were produced by other sources, including diopside, monticellite, and akermanite, during the firing process of dolomite-rich clay. A collection of gehlenite, wollastonite, and larnite was detected in the calcium-rich clay. Diopside, akermanite, forsterite, periclase, monticellite, and spinel were observed in the reaction products of the magnesium (calcium)-rich clay. The presence of a potassium–calcium sulfate was recognized in both clays fired between 900 and 1100 °C [33].

The present study explores the possibility of reducing the cost of magnesia refractories by adding clay and fireclay. The main objective is to investigate the effects of adding clay and fireclay to magnesite on the formation and properties of magnesia–forsterite–spinel refractories.

2. Materials and methods

Clay and fireclay were chosen as additives to be introduced to magnesite. The raw materials were ground in an alumina jar mill and were passed through a 45-μm sieve before determining their chemical and phase compositions. The chemical composition of the raw materials was determined through an X-ray fluorescence spectrometer (XRF: ARL 8410 with Rh radiation, 40 mA, 60 kV) under normal conditions. Table 1 presents the results of the chemical analysis of the starting materials.

An X-ray diffractometer (XRD: Siemens D-500 with CuKα radiation, 30 mA, 40 kV) was used to investigate the phase composition of the raw materials and phase evolution in the processed samples. The XRD results were analyzed with the aid of the X'Pert HighScore software. Table 2 shows the results of the phase analysis of the staring materials.

Table 3 shows the initial constituents of the samples and the defined coding system. The samples were prepared by first calcining the clay at 800 °C and then grinding in the alumina ball mill. The fireclay and magnesite were also ground for 8 h to obtain a suitable PSD. The batches were treated in the distilled water solution to enhance their mixability. Then, they were mixed for 1 h and dried overnight in an oven at 120 °C. The dried samples were used to make granules with 4% moisture for pressing. 10 g of each batch was weighted for the preparation of bars with dimensions of 60×10×5 mm^3 utilizing uniaxially pressing with a load of 100 MPa. The samples were fired at 1350, 1450, and 1550 °C in an electric kiln with a rate of 5 °C/min and were soaked for 4 h at a maximum temperature under atmospheric conditions.

The shrinkage of the 27 samples (9 formulations fired at 3 different temperatures) was determined by direct measuring the length of the samples with a caliper. Meanwhile, their porosity was determined using the Archimedes method. A scanning electron microscope (SEM: Cambridge Stereoscan 360) was employed to study the microstructural characteristics of the produced samples. Particle size distribution (PSD) and flexural strength were determined by a particle size analyzer (Fritsch Analysette 22) and a three-point bending strength test machine (Instron 1196), respectively.

3. Results and discussion

3.1. Phase analysis

Due to the similarity of the samples composition and to decrease the cost of the characterizations, only a limited number of them underwent phase analysis. Fig. 1 shows the XRD patterns of samples 3-1350,

Table 2. Phase composition of starting materials.

Starting materials	Phase composition
Magnesite	Periclase
Clay	Silica, kaolinite, nacrite, and illite
Fireclay	Mullite and cristobalite

Table 3. Coding system and initial constituents of the samples.

Initial formulation (wt%)	Sample code								
	1-T*	2-T	3-T	4-T	5-T	6-T	7-T	8-T	9-T
Magnesite	100	95	90	85	80	90	80	70	60
Clay	0	5	10	15	20	0	0	0	0
Fireclay	0	0	0	0	0	10	20	30	40

* T stands for temperature in °C: 1350, 1450 or 1550

3-1450, and 3-1550 fired at different temperatures, as well as sample 6-1450. As expected, the semi-quantitative analysis revealed that the major phase in the samples is periclase.

The main recognized phases in the samples after sintering were periclase and forsterite. Although some alumina (about 15% according to Table 1) was present in the initial clay composition, the XRD patterns of samples 3-1350, 3-1450, and 3-1550 exhibited no alumina phase. Thus, aluminum oxide might have been solved in other phases and formed a solid solution. Of course, it should be noted that the amount of clay in the initial formulation of series 3-T samples was only 10%. Hence, the amount of alumina may have been so small that it was beyond the ability of the XRD analyzer to be detected.

Another important point is the absence of the mullite phase in the XRD patterns of sintered samples. According to the calcia/silica molar ratio, the aluminosilicate compounds were probably consumed during the evolution of forsterite and spinel phases. Fig. 1 shows that spinel is not present in the samples containing clay as an additive. However, spinel was synthesized in sample 6-1450, the additive of which was fireclay.

3.2. Porosity, bulk density, and shrinkage

Fig. 2 shows the porosity of the samples fabricated at different firing temperatures as a function of clay content. As expected, sintering at higher temperatures decreases the porosity in the samples. The standard deviations of the porosity of the samples suggest that nearly no significant changes in porosity occurred when clay was added to magnesia. Anyway, in the samples manufactured at 1350 °C, the porosity variations have a sinusoidal behavior between ~25% and ~29%. In samples sintered at 1450 °C, the porosity increases from ~23% for the clay-free sample to ~26% for the sample containing 10% clay, but adding more clay up to 20% reduces the porosity to ~22%. In samples fabricated at 1550 °C, the addition of clay up to 10% has little effect on the porosity as the porosity is ~21% constant. Adding more clay to 20% reduces the porosity to less than 18%.

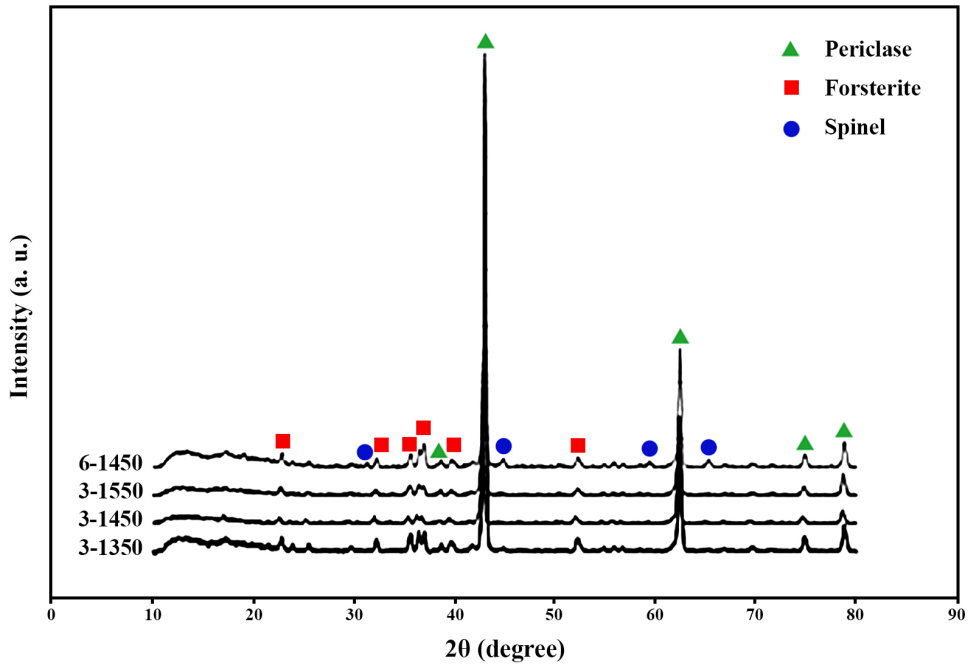

Fig. 1. XRD patterns of samples 3-1350, 3-1450, 3-1550, and 6-1450.

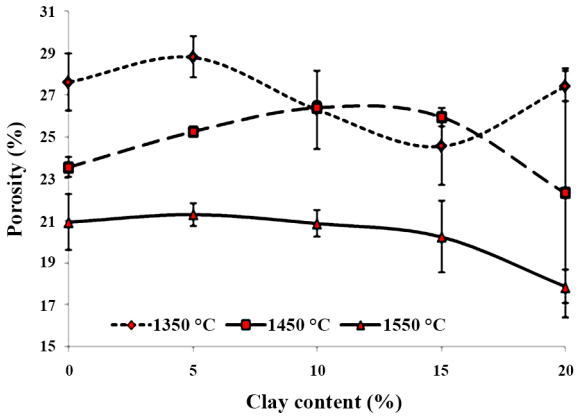

Fig. 2. Porosity of the samples sintered at different temperatures as a function of clay content.

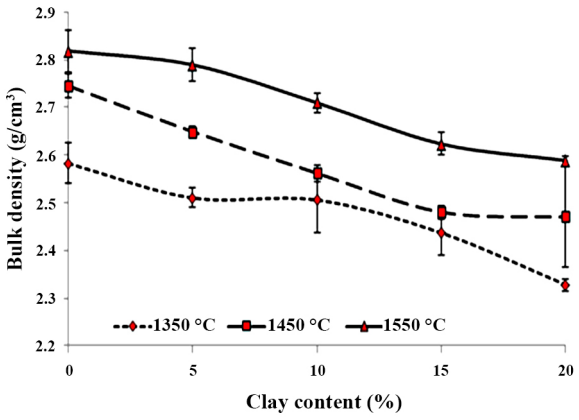

Fig. 4. Bulk density of the samples sintered at different temperatures as a function of clay content.

As clearly seen in Fig. 3, adding fireclay affected the porosity content in the sintered magnesia. It seems that at all sintering temperatures, increasing the amount of fireclay initially reduces the amount of porosity, but with further increase of this additive, the amount of porosity sharply increases. The lowest porosity was obtained by adding 20% fireclay in the samples sintered at 1450 and 1550 °C. However, in the samples made at 1350 °C, the lowest porosity was observed in the specimen containing 10% fireclay. As expected from these experiments, the sintering temperature has a significant effect on the densification process, and as the temperature increases, the porosity decreases remarkably.

Given that the porosity contents of the fired samples with clay additive have not markedly changed, the slight decrease in bulk density values caused by adding clay, as shown in Fig. 4, may be attributed to the differences in density of clay (2.86 g/cm^3) [34] and magnesite (3.23 g/cm^3) [35]. Such an attribution is supported by the nearly constant shrinkage of the samples with various amounts of clay, as illustrated in Fig. 5. However, both the bulk density and shrinkage variations of the samples generally show an almost linear decreasing behavior with increasing clay content. Moreover, Figs. 5 and 6 clearly show the effective role of the firing temperature in increasing the bulk density and shrinkage of the samples.

Figs. 6 and 7 present the bulk density and shrinkage of the samples, respectively, sintered at different temperatures as a function of fireclay content. As can be expected, the bulk density and shrinkage of the samples increased with increasing the sintering temperature. In the samples processed at 1350 °C, the addition of fireclay up to 10% did not affect the bulk density, but the addition of higher amounts of this additive caused a significant drop in bulk density. In the samples made at 1450 °C, the addition of fireclay up to 20% caused a very small decrease in bulk density, but the introduction of more additive caused a sharp drop in this property. At the firing temperature of 1550 °C, it seems that adding 10% of fireclay increases the bulk density, but similar to other temperatures, more additives cause a bulk density drop.

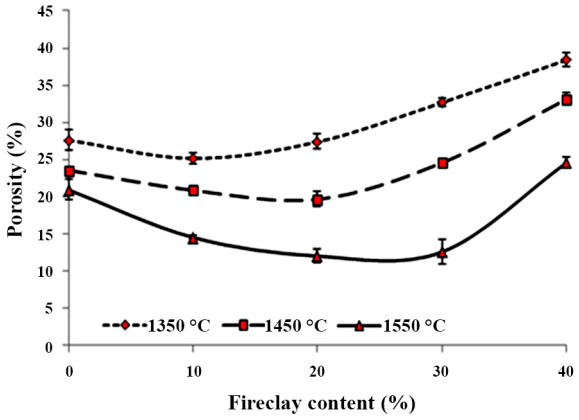

Fig. 3. Porosity of the samples sintered at different temperatures as a function of fireclay content.

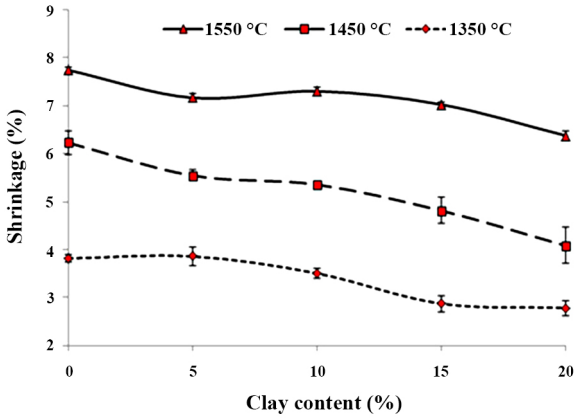

Fig. 5. Shrinkage in the samples sintered at different temperatures as a function of clay content.

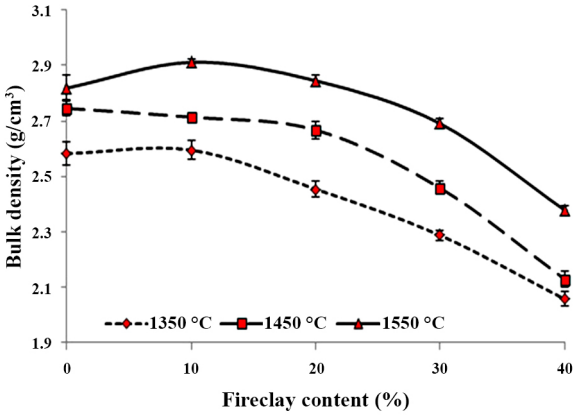

Fig. 6. Bulk density of the samples sintered at different temperatures as a function of fireclay content.

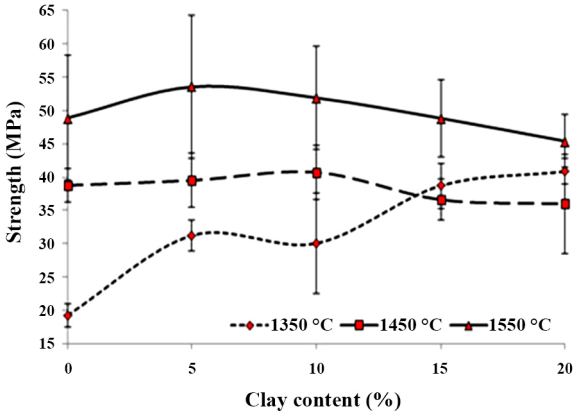

Fig. 8. Bending strength of the samples sintered at different temperatures as a function of clay content.

In shrinkage graphs (Fig. 7) of the samples with fireclay additive, with increasing the amount of this additive, the shrinkage first increases, but with increasing the amount of additive, this property decreases. The maximum shrinkage was obtained by adding 10% of fireclay in the samples processed at 1350 and 1450 °C, but at the sintering temperature of 1550 °C, the highest shrinkage belonged to the sample containing 20% fireclay.

3.3. Bending strength

Figs. 8 and 9 show the changes in the bending strength values of the samples processed at different temperatures as a function of clay and fireclay contents, respectively. As can be seen in both figures, increasing the fabrication temperature of the specimens has led to greater flexural strength. These observations may be attributed to the decrease in porosity content, which resulted in better bonding between the grains in samples fired at higher temperatures. According to Fig. 8, the addition of more clay in the samples processed at 1350 °C has improved the flexural strength as much as possible. However, in the samples made at higher temperatures, it seems that the addition of clay did not have much effect on the flexural strength of the samples. The trends of changes in the flexural strength of the samples containing fireclay have sinusoidal behaviors. Due to the considerable values of the measured standard deviations, the effect of this additive on the strength of the resulting material cannot be judged accurately and correctly.

3.4. Microstructure observation

Fig. 10 shows the microstructures of the samples with 10% clay additive sintered at different temperatures. The growth of crystals can be observed by increasing the firing temperature. The necks are increasingly formed, so the increase in the bending strength at higher temperatures is confirmed. No trace of liquid phase formation was seen in the SEM images, so the hypothesis that the sintering process in this system has progressed in the solid state is strengthened and proven.

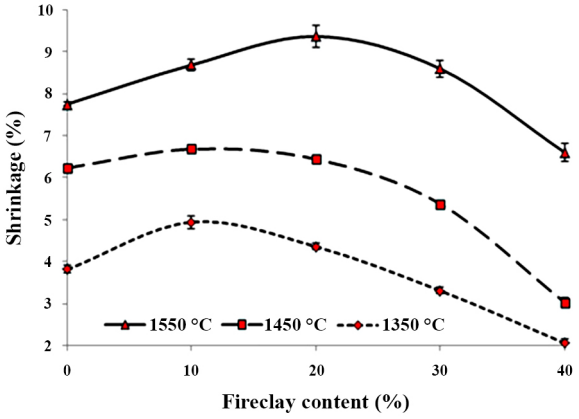

Fig. 7. Shrinkage in the samples sintered at different temperatures as a function of fireclay content.

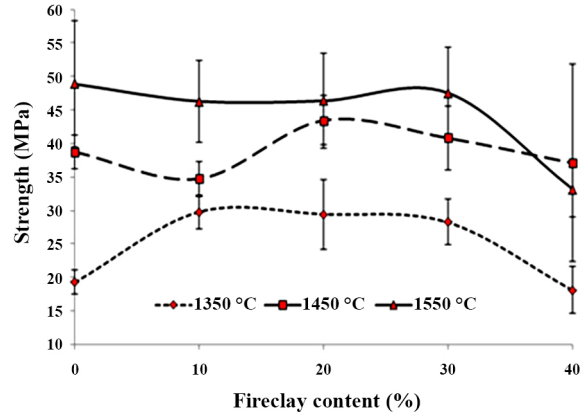

Fig. 9. Bending strength of the samples sintered at different temperatures as a function of fireclay content.

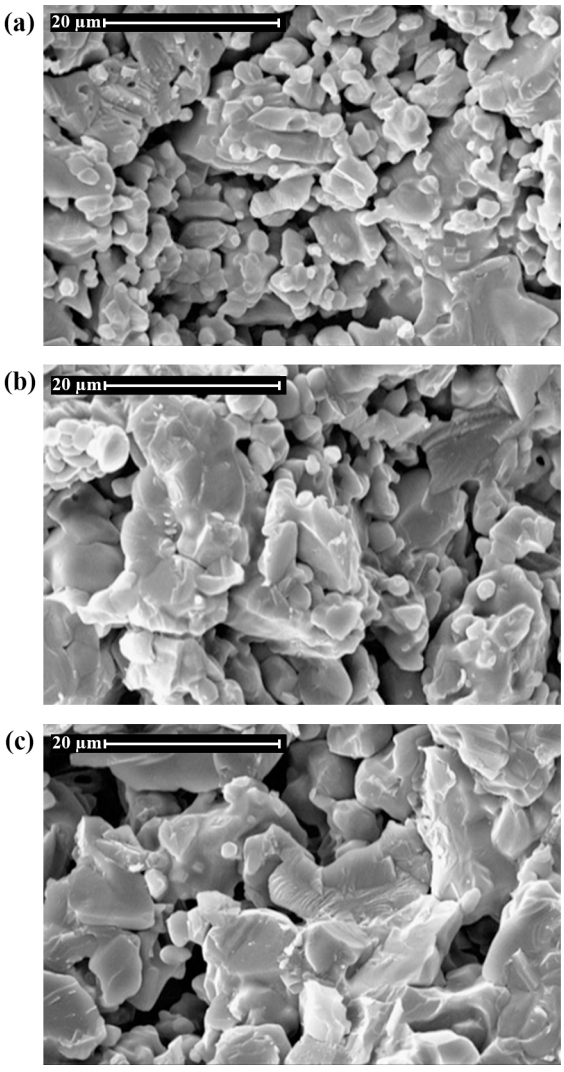

Fig. 10. Microstructure of the samples with 10% clay additive sintered at different temperatures: a) 3-1350, b) 3-1450, and c) 3-1550.

4. Conclusions

Given the experimental results of this study, the following conclusions can be drawn:

- Phase analysis showed that adding fireclay to magnesite caused the synthesis of forsterite and spinel, whereas adding clay primarily led to the evolution of forsterite.
- Sintering at higher temperatures increased the shrinkage and decreased the porosity content.
- Increasing the amounts of clay or fireclay additives did not significantly affect the bending strength.
- Despite the occurrence of grain growth at higher temperatures, increased bonding among the particles, resulted in enhanced bending strength.
- Determining the optimal amount of fireclay or clay based on the cost of the final product requires additional research and characterizations.

CRediT authorship contribution statement

Esmaeil Salahi: Project administration, Resources, Supervision.
Mehran Ghaffari: Methodology, Writing – original draft.
A. Faeghinia: Investigation, Writing – original draft.
Armin Rajabi: Data curation, Writing – review & editing.

Data availability

The data underlying this article will be shared on reasonable request to the corresponding author.

Declaration of competing interest

The authors declare no competing interests.

Funding and acknowledgment

The authors would like to extend their gratitude to the Materials and Energy Research Center and Universiti Kebangsaan Malaysia for their support of this research.

References

[1] M. Mansoor, M. Mansoor, M. Mansoor, T. Themelis, F. Çinar Şahin, Sintered transparent polycrystalline ceramics: the next generation of fillers for clarity enhancement in corundum, Synth. Sinter. 1 (2021) 183–188. https://doi.org/10.53063/synsint.2021.1342.
[2] W. Zhang, S. Song, M. Nath, Z. Xue, G. Ma, Y. Li, Inhibition of Cr6+ by the formation of in-situ Cr3+ containing solid-solution in Al2O3–CaO–Cr2O3–SiO2 system, Ceram. Int. 47 (2021) 9578–9584. https://doi.org/10.1016/j.ceramint.2020.12.092.
[3] A. Valenzuela-Gutiérrez, J. López-Cuevas, A. González-Ángeles, N. Pilalua-Díaz, Addition of ceramics materials to improve the corrosion resistance of alumina refractories, SN Appl. Sci. 1 (2019) 784. https://doi.org/10.1007/s42452-019-0789-5.
[4] A. Faeghinia, Impact of bridging oxygens formation on optical properties of Fe3+ doped Li2O–Al2O3–SiO2–TiO2 glasses, Synth. Sinter. 2 (2022) 14–19. https://doi.org/10.53063/synsint.2022.2179.
[5] P. Das, S. Sinhamahapatra, K. Dana, S. Mukhopadhyay, Improvement of thermal conductivity of carbonaceous matrix in monolithic Al2O3–C refractory composite by surface-modified graphites, Ceram. Int. 46 (2020) 29173–29181. https://doi.org/10.1016/j.ceramint.2020.08.090.
[6] A.G.M. Othman, Effect of talc and bauxite on sintering, microstructure, and refractory properties of Egyptian dolomitic magnesite, Br. Ceram. Trans. 102 (2003) 265–271. https://doi.org/10.1179/096797803225009391.
[7] F. Boenzi, Possible ecological advantages from use of carbonless magnesia refractory bricks in secondary steelmaking: a framework LCA perspective, Int. J. Environ. Sci. Technol. 19 (2022) 5877–5896. https://doi.org/10.1007/s13762-021-03553-2.
[8] L. Xu, M. Chen, N. Wang, S. Gao, Chemical wear mechanism of magnesia-chromite refractory for an oxygen bottom-blown copper-smelting furnace: A post-mortem analysis, Ceram. Int. 47 (2021) 2908–2915. https://doi.org/10.1016/j.ceramint.2020.09.124.
[9] P. Yang, G. Xiao, D. Ding, Y. Ren, S. Yang, et al., Antioxidant properties of low-carbon magnesia-carbon refractories containing AlB2–Al–Al2O3 composites, Ceram. Int. 48 (2022) 1375–1381. https://doi.org/10.1016/j.ceramint.2021.09.223.
[10] Y. Mi, Y. Xu, Y. Li, S. Sang, Q. Wang, Fabrication and thermal shock behavior of ZrO2 toughened magnesia aggregates, Ceram. Int. 47 (2021) 26475–26483. https://doi.org/10.1016/j.ceramint.2021.06.060.

[11] N.V. Buchilin, V.Y. Nikitina, A.A. Lugovoi, N.M. Varrik, V.G. Babashov, Preparation of alumina-magnesia spinel based high-porosity ceramic materials, Glas. Ceram. 77 (2021) 372–378. https://doi.org/10.1007/s10717-021-00310-2.
[12] Y. Dai, C. Wu, Study on properties of magnesium phosphosilicate cement using different reactive magnesia, J. Ceram. Soc. Jpn. 129 (2021) 540–550. https://doi.org/10.2109/jcersj2.21022.
[13] S. Xuan, X. Wang, Y. Tian, J. Hao, Properties of magnesium-aluminate spinel derived from bauxite and magnesia, Int. J. Appl. Ceram. Technol. 18 (2021) 1205–1212. https://doi.org/10.1111/ijac.13740.
[14] F. Gu, Z. Peng, Y. Zhang, H. Tang, L. Ye, et al., Thermodynamic characteristics of ferronickel slag sintered in the presence of magnesia, The Minerals, Metals & Materials Series, Springer, Cham. (2019) 379–388. https://doi.org/10.1007/978-3-030-05749-7_38.
[15] K. Li, F. Zhao, X. Liu, H. Mai, E. Xu, et al., Fabrication of porous forsterite-spinel-periclase ceramics by transient liquid phase diffusion process for high-temperature thermal isolation, Ceram. Int. 48 (2022) 2330–2336. https://doi.org/10.1016/j.ceramint.2021.10.012.
[16] Z. Peng, L. Yuan, X. Luo, J. Yu, C. Tian, Z. Liu, Mechanical properties and thermal shock resistance performance of spark plasma sintered MgO–Al2O3–SiO2 ceramics, Ceram. Int. 48 (2022) 28548–28556. https://doi.org/10.1016/j.ceramint.2022.06.168.
[17] X. Ren, B. Ma, G. Fu, F. Qian, G. Liu, et al., Facile synthesis of MgO–Mg2SiO4 composite ceramics with high strength and low thermal conductivity, Ceram. Int. 47 (2021) 19959–19969. https://doi.org/10.1016/j.ceramint.2021.03.331.
[18] M. Nguyen, R. Sokolář, Thermal and thermomechanical properties of refractory forsterite-spinel ceramics, Solid State Phenom. 325 (2021) 174–180. https://doi.org/10.4028/www.scientific.net/SSP.325.174.
[19] M. Nguyen, R. Sokolář, Corrosion resistance of novel fly ash-based forsterite-spinel refractory ceramics, Materials (Basel). 15 (2022) 1363. https://doi.org/10.3390/ma15041363.
[20] F. Zhao, L. Zhang, Z. Ren, J. Gao, X. Chen, et al., A novel and green preparation of porous forsterite ceramics with excellent thermal isolation properties, Ceram. Int. 45 (2019) 2953–2961. https://doi.org/10.1016/j.ceramint.2018.09.296.
[21] H. Liu, C. Jie, Y. Ma, Z. Wang, X. Wang, Synthesis and processing effects on microstructure and mechanical properties of forsterite ceramics, Trans. Indian Ceram. Soc. 79 (2020) 83–87. https://doi.org/10.1080/0371750X.2020.1722754.
[22] J. Nishizawa, T. Ikeda-Fukazawa, Surface structures and properties of forsterite in crystalline and glassy states, Chem. Phys. Lett. 714 (2019) 197–201. https://doi.org/10.1016/j.cplett.2018.11.014.
[23] Y. Zou, H. Gu, A. Huang, Y. Huo, L. Fu, Y. Li, Characterisation and properties of low-conductivity microporous magnesia based aggregates with in-situ intergranular spinel phases, Ceram. Int. 47 (2021) 11063–11071. https://doi.org/10.1016/j.ceramint.2020.12.229.
[24] S. Lamara, D. Redaoui, F. Sahnoune, M. Heraiz, N. Saheb, Microstructure, thermal expansion, hardness and thermodynamic parameters of cordierite materials synthesized from Algerian natural clay minerals and magnesia, Bol. Soc. Esp. Cerám. Vidr. 60 (2021) 291–306. https://doi.org/10.1016/j.bsecv.2020.03.008.
[25] Z. Quan, Z. Wang, X. Wang, H. Liu, Y. Ma, Effects of Sm2O3 addition on sintering behavior of pre-synthesized magnesia-rich magnesium aluminate spinel, J. Rare Earths. 39 (2021) 1450–1454. https://doi.org/10.1016/j.jre.2021.01.020.
[26] S.S. Hossain, P.K. Roy, Preparation of multi-layered (dense-porous) lightweight magnesium-aluminum spinel refractory, Ceram. Int. 47 (2021) 13216–13220. https://doi.org/10.1016/j.ceramint.2021.01.076.
[27] F.G. Khomidov, Z.R. Kadyrova, K.L. Usmanov, S.M. Niyazova, B.T. Sabirov, Peculiarities of sol-gel synthesis of aluminum-magnesium spinel, Glass Ceram. 78 (2021) 251–254. https://doi.org/10.1007/s10717-021-00389-7.
[28] F.N. Cunha-Duncan, R.C. Bradt, Synthesis of Magnesium Aluminate Spinels from Bauxites and Magnesias, J. Am. Ceram. Soc. 85 (2004) 2995–3003. https://doi.org/10.1111/j.1151-2916.2002.tb00569.x.
[29] N. Petric, V. Martinac, E. Tkalcec, H. Ivankovic, B. Petric, Thermodynamic analysis of results obtained by examination of the forsterite and spinel formation reactions in the process of magnesium oxide sintering, Ind. Eng. Chem. Res. 28 (1989) 298–302. https://doi.org/10.1021/ie00087a008.
[30] V.A. Perepelitsyn, Y.I. Savchenko, V.M. Bezhaev, S.N. Tabatchikova, Petrochemical calculations in the production of forsterite-spinel refractories from carbon ferrochrome slags, Refractories. 27 (1986) 568–572. https://doi.org/10.1007/BF01387278.
[31] N.M. Khalil, Refractory aspects of Egyptian alum-waste material, Ceram. Int. 27 (2001) 695–700. https://doi.org/10.1016/S0272-8842(01)00022-0.
[32] A.G.M. Othman, N.M. Khalil, Sintering of magnesia refractories through the formation of periclase–forsterite–spinel phases, Ceram. Int. 31 (2005) 1117–1121. https://doi.org/10.1016/j.ceramint.2004.11.011.
[33] M.J. Trindade, M.I. Dias, J. Coroado, F. Rocha, Mineralogical transformations of calcareous rich clays with firing: A comparative study between calcite and dolomite rich clays from Algarve, Portugal, Appl. Clay Sci. 42 (2009) 345–355. https://doi.org/10.1016/j.clay.2008.02.008.
[34] P. Schjønning, R.A. McBride, T. Keller, P.B. Obour, Predicting soil particle density from clay and soil organic matter contents, Geoderma. 286 (2017) 83–87. https://doi.org/10.1016/j.geoderma.2016.10.020.
[35] Y. Zou, H. Gu, A. Huang, L. Fu, G. Li, et al., Pore evolution of microporous magnesia aggregates with the introduction of nano-sized MgO, Ceram. Int. 48 (2022) 18513–18521. https://doi.org/10.1016/j.ceramint.2022.03.121.